PERGAMON

Journal of Structural Geology 21 (1999) 323–334

JOURNAL OF STRUCTURAL GEOLOGY

Micro-shear zones in experimentally deformed octachloropropane

Paul D. Bons *, Mark W. Jessell

Department of Earth Sciences, Monash University, Clayton, Melbourne 3168, Australia

Received 6 June 1997; accepted 1 September 1998

Abstract

Localisation of deformation in rocks is known to be important at all scales in ductily deforming rocks. However, relatively little is known of the significance of shear localisation at small scales (< mm–cm), where ongoing deformation and recovery may obliterate any traces of such localisation.

We investigated localisation of deformation in a < 100 μm thick sample of the rock analogue octachloropropane in a transparent torsional deformation cell with a circular shear zone in which arbitrarily high values of simple shear can be achieved. Photomicrographs of the deforming sample were taken every 1–2 min over eight and five minute intervals, while the sample was deforming at a bulk shear-strain rate of $4.6\times10^{-4}\,s^{-1}$, after a steady-state microstructure was established. The distribution of deformation was determined using pattern matching on digitised photomicrographs.

Localisation of deformation was observed in the form of anastomosing micro-shear zones on the grain and sub-grain scale (10–100 μm). These shears left no clear indicative microstructures. The micro-shear zones shifted through the material, partly along with migrating grain boundaries, causing a homogenisation of accumulated strain. The existence of such micro-shear zones can therefore not be determined easily by microstructural analysis of deformed material, even though in these experiments the micro-shear zones accommodated up to 75% of the total deformation.

A second form of localisation, which occurs at the inside and outside of the shear zone and which is often observed in this type of experiment, was also noted, and can be accounted for by the friction between the sample and the confining glass plates.

1. Introduction

Localisation of deformation is the norm rather than the exception in ductily deforming rocks. Two well studied examples of this localisation are, for instance, planar shear zones and *S–C* fabrics (Berthé et al., 1979; White et al., 1980; Hanmer and Passchier, 1991; Ishii, 1992). These forms of shear localisation occur on the scale of mm to tens of metres and are readily observed in outcrop or hand specimen by the internal microstructures (e.g. mylonitic texture) or offset markers (e.g. layering or dykes). Much less is known about the distribution and possible localisation of deformation on smaller scales. The main problem here is that sub-mm scale structures are easily obliterated or reset by ongoing deformation and syn-tectonic or post-tectonic metamorphism (Means, 1981; Lister and Snoke, 1984; Urai et al., 1986; Ree, 1991; Ree and Park, 1997).

There are several reasons to expect shear localisation to develop at the sub-grain and grain scale: (1) shear localisation is normal at all larger scales; (2) rocks are mechanically heterogeneous down to the sub-grain level, due to differences in properties of different minerals, and due to differences in mechanical response to deformation of grains with respect to the orientation of crystal lattices (Wenk et al., 1986); and (3) the response of most ductile materials to deformation favours the development of instabilities and hence localisation of deformation (Poirier, 1980; Hobbs et al., 1986; Hobbs and Ord, 1988).

Shear localisation down to the sub-mm scale has been studied in natural rocks (Platt and Vissers, 1980; Gapais and White, 1982; Platt, 1984), but smaller scale shear localisation at any one site in a deforming rock can be expected to be short-lived or spatially transient due to the ongoing (deformation-induced) recrystallisation. Micro-scale shear localisation is therefore usually

* Corresponding author. E-mail: paul@earth.monash.edu.au. Now at: Institut für Geowissenschaften–Tektonophysik, Universität Mainz, Becherweg 21, 55099 Mainz, Germany, E-mail: bons@mail.uni-mainz.de

0191-8141/99 $ - see front matter
PII: S0191-8141(98)00116-3

difficult to observe in natural rocks, but has been observed and described in experiments (Drury et al., 1985; Drury and Humphreys, 1988; Ree, 1994; Herwegh and Handy, 1996).

The experimental deformation of rock analogues in transparent deformation cells is ideally suited to study the deformation distribution in deforming crystalline materials (Means, 1989). In these experiments a thin sample is deformed between two glass plates to allow continuous observation with a microscope. If materials are chosen with low melting temperatures, one can achieve very high shear strains (up to hundreds) in a matter of days at low (room) temperature and stress. Continuous observation facilitates determination of the distribution of deformation at any stage during progressive deformation (Bons et al., 1993; Bons and Jessell, 1995). Using the high-resolution strain analysis technique of Bons and Jessell (1995), we describe microscopic scale shear zones in a polycrystalline organic rock analogue, octachloropropane.

2. Experimental procedure

One experiment was performed at room temperature with a torsional transparent deformation cell similar to those used by Jessell and Lister (1991) and ten Brink and Passchier (1995) (Fig. 1). A sample, less than about 100 μm thick, is deformed between two glass plates. The lower plate has a circular roughened or frosted patch with a radius of 2.11 mm in the centre, while the upper plate has a centred frosted ring on it with an inner radius of 5.25 mm. The upper plate is rotated at a speed of one full rotation per 6.4 h with respect to the fixed lower plate. The rotation is driven by a geared-down stepper motor, which has a very constant rate determined by the 50 Hz mains frequency. The resulting deformation geometry is that of a circular 3.14 mm wide simple shear zone, where the outer edge moves at a velocity of 1.43 μm/s. The rotation of the upper glass plate is unlimited and arbitrarily high shear strains can therefore be achieved. The load applied by the motor was not recorded. The total duration of the experiment was 50 h, in which a bulk shear strain (total displacement of outer grip divided by width of shear zone) of 81 was achieved. The microstructural developments were monitored with a microscope during the experiment and a total of 350 black and white micrographs were taken on a 35 mm film. Two sequences of micrographs were chosen for further analysis: one at 24 h at a bulk shear strain of 39 for analysis of shear distribution across the whole shear zone and one after 27 h at a bulk shear strain of 43 for analysis of a small area near the inner edge of the shear zone. It was observed that at that stage a steady-state microstructure was well established.

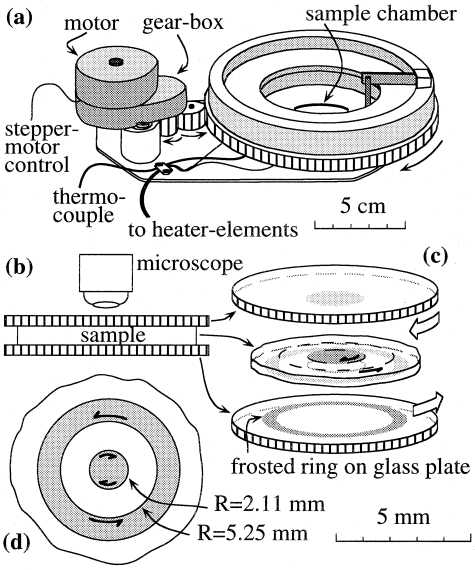

Fig. 1. (a) Drawing of the transparent deformation cell. (b) Inside the sample chamber, a thin (≤100 μm) sample is sandwiched between two glass plates and can be viewed with a microscope. (b) Each glass plate has a ring frosted on it. (c) These frosted rings grip the sample and make it deform when the glass plates are rotated in opposite directions. (d) The resulting deformation is that of a circular shear zone. 'R' refers to the radii of the inside and outside of the shear zone.

Octachloropropane (C_3Cl_8, abbreviated to OCP) was used in the experiment. It is an organic crystalline material that melts at 160°C and deforms ductily at room temperature, atmospheric pressure and low stresses (< 1 MPa) (McCrone and Cheng, 1949; Jessell, 1986). A power-law relationship between strain rate and stress was observed by Bons and Urai (1994) with a stress exponent of 4.5 at 30°C. The experiment described here was performed at this temperature (a homologous temperature of 0.7).

About one volume percent of fine aluminium powder was thoroughly mixed in with the OCP in order to determine the displacements of material points during (small) strain increments. Ninety-five percent of the particles were less than 20 μm in diameter, but a few particles were larger, up to 100 μm in length. Grain-boundary migration appears to be generally not hindered by the presence of particles, even in the case of static recovery (Bons and Urai, 1992; Ree and Park, 1997). As the driving forces for dynamic recrystallisation are much higher than for static recovery (Urai et al., 1986), we assume that the small fraction of marker particles has a negligible effect on the microstructural development and rheology of the OCP. Displacements of marker particles were determined with pattern matching software (Bons and Jessell, 1995). The distribution of deformation during a strain increment can then be derived from the displacements (Ramberg, 1975; Mancktelow, 1991; Bons et al., 1993).

3. Grain scale shear zones in polycrystalline OCP

3.1. Results

The sample of polycrystalline OCP was deformed to a total strain of 81. Shear was localised near the edges of the shear zone at all times. This is an artefact of the experimental technique and is discussed in the next section. For this part of the study we focus on the deformation over an eight minute time interval in a small area near the inner edge of the shear zone (Fig. 2). The bulk shear strain at the beginning of the interval was about 43, but would be more than 100 in the selected area, due to shear localisation at the edge of the shear zone. The actual value of finite strain is by then irrelevant, since a steady-state microstructure has long since been established as well as a steady-state crystallographic preferred orientation, with two *c*-axis point maxima, resulting in the basal planes and prismatic planes being approximately parallel to the shear plane.

The distribution of deformation accumulated over the 8 min interval was calculated from plane polarised light images (Fig. 2c and d) with the pattern-matching routine of Bons and Jessell (1995). The resolution is about 10 μm, depending on the density and pattern in the marker particles. The results are shown in the form of a deformed grid in Fig. 3(a). The strongest deformation is found near the edge of the shear zone at the bottom of the image where deformation is so intense

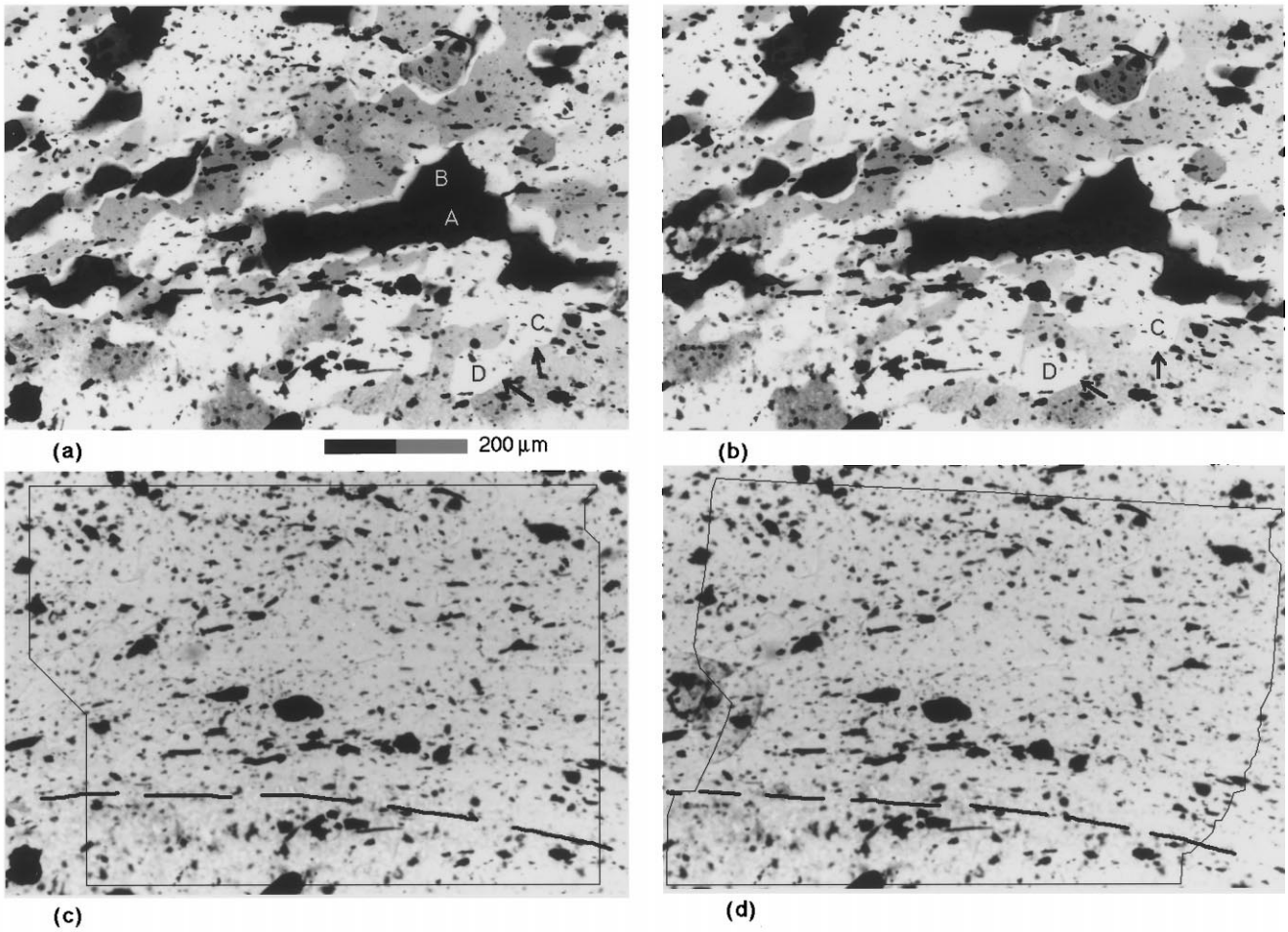

Fig. 2. Micrographs of the area selected for strain analysis at the edge of the dextral shear zone. (a) OCP under crossed polarised light at the beginning of the selected deformation interval. Dark grains have basal planes in the plane of the image. Most other grains have their basal planes close to the approximately horizontal shear plane. Grains A and B are in the centre of the area shown in Fig. 4. (b) Same area under crossed polarised light 8 min later. Deformation at the edge of the inner grip can be seen by the tearing apart of grains C and D (arrows in the lower right corner), accompanied by grain boundary migration. (c) Same area under plane polarised light at the beginning of the selected deformation interval. Black dots and specks are the aluminium powder particles used for the strain analysis. Dashed line shows the edge of the shear zone at the inner frosted grip. The outer grip is not in the field of view. The extent of the analysed area is outlined with a thin black line. (d) Same area at the end of the deformation interval, 8 min later, with the now deformed outline of the analysis area drawn over it. Micrographs are digitised using a flat bed scanner from 13×18 cm prints, printed from 35 mm black and white negatives. The images are 700 pixels wide.

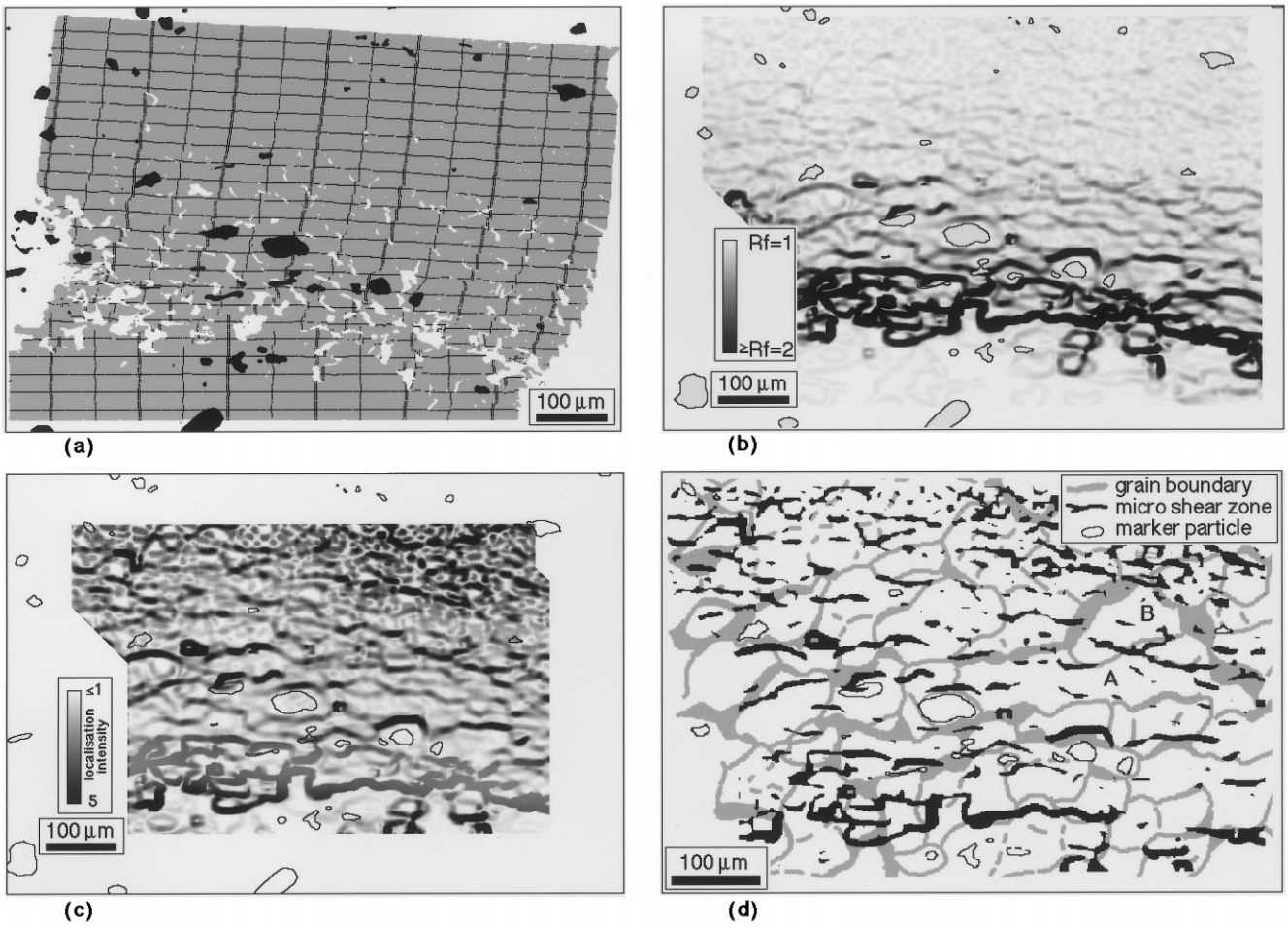

Fig. 3. Results of the analysis of the deformation in the area shown in Fig. 2. (a) Deformation distribution visualised with a deformed grid, constructed by applying the measured displacement field to an imaginary grid (see Fig. 2c for original outline of this grid). Dextral shear is clearly localised at the inner edge of the shear zone. The vertical grid bands are often off-set in small steps, signifying deformation by micro-shear zones. White patches are a result of dilatancy or of failure of the pattern matching routine when deformation is too intense. Black dots are some of the aluminium powder particles. (b) Grey-scale plot of R_f: the axial ratio of the finite strain ellipse. R_f was calculated from a least-squares best fit of homogeneous deformation to the displacement data in a 10×10 pixel window around each point in the image. Dark 'worms' are zones of strongest deformation. (c) The same image as (b), normalised by the background R_f value, calculated with a 100×100 pixel window, giving a measure of the localisation intensity. This image also highlights the micro-shear zones away from the high deformation zone at the edge of the shear zone. (d) Overlay of the micro-shear zones (all areas in (c) with a value $R_f > 2.5$ drawn in black) and the grain boundaries (light grey, drawn after Fig. 2a). Many, but not all of the micro-shear zones are located at or near grain boundaries. Arrows point at some examples. Note that grain boundaries can be oblique to the glass plates and appear very wide and that not all grain boundaries can be picked up or distinguished from sub-grain boundaries in a single black and white micrograph. The positions of points and aluminium powder particles in (b), (c) and (d) are those at the beginning of the deformation interval.

that the pattern-matching routine for strain analysis becomes unreliable. Here, and in the lower strain rate area further away from the grip, deformation is concentrated in narrow anastomosing zones. The width of many of these shear zones appears to be one or two pixels or ≤ 2 µm, which is less than the resolution of about 10 µm. These shear zones are thus at most 10 µm wide.

The distribution of incremental finite strain was calculated and is shown in Fig. 3(b) as grey-scale images of the axial ratio (R_f) of the finite strain ellipse. R_f can be calculated from the position gradient tensor (Passchier, 1988; Means, 1990), which was calculated with a least-squares best fit of homogeneous deformation to the displacement values in a window of 10×10 pixels (12×12 µm) around each point in the image. Since there is an overall gradient in strain rate over the whole area, due to localisation near the grip, it is also of interest to visualise the intensity of strain relative to the background value. The background R_f-values were calculated with a 100×100 pixel window least-squares fit. The relative R_f or localisation intensity L was then calculated with:

$$L = \frac{R_{f_{(10\times10\text{ window})}} - 1}{R_{f_{(100\times100\text{ window})}} - 1} \quad (1)$$

The results are shown in Fig. 3(c), highlighting the small shear zones in the lower strain area in the upper half of the image. Finally, it is of interest to see how the distribution of the micro-shear zones relates to the microstructure. Fig. 3(d) shows an overlay of the highest localisation intensities and traces of the grain boundaries. One can see that there is some control by the grain and sub-grain boundaries on the distribution of micro-shear zones, but micro-shear zones can also cut through grains. Because the shear localisation is preferentially located at grain boundaries, this type of deformation could be termed grain-boundary sliding. We prefer however not to use this term, since it is usually used for deformation where each grain slides past its neighbours. The micro-shear zones observed here are different in that they let small lenses slide past each other and may cut through grains. Each lens may range from one sub-grain to several grains in size.

A more detailed and higher resolution analysis was performed on a smaller region (Fig. 4a) around grains A and B in Fig. 2(a). The deformed grid (Fig. 4b) clearly shows that deformation is inhomogeneous, with the micro-shear zones off-setting the original vertical grid lines in several steps. Most offsets are less than 10 μm, with the exception of the lower left corner where deflection of shear around a large aluminium oxide particle produces an offset of about 25 μm. White areas within the deformed grid are dilatant zones.

These zones are not visible in the microstructure as voids or cracks (as in Ree, 1994) and are interpreted to be the product of local addition of OCP by diffusional material transfer. It was considered that shearing in the OCP parallel to the glass plate could lead to apparent dilatant zones. If some marker particles lie close to one glass plate and others lie close to the other glass plate, apparent dilatant zones may appear as these particles can move apart. As the marker particles are randomly distributed through the sample, such apparent dilatant zones and their counterparts,

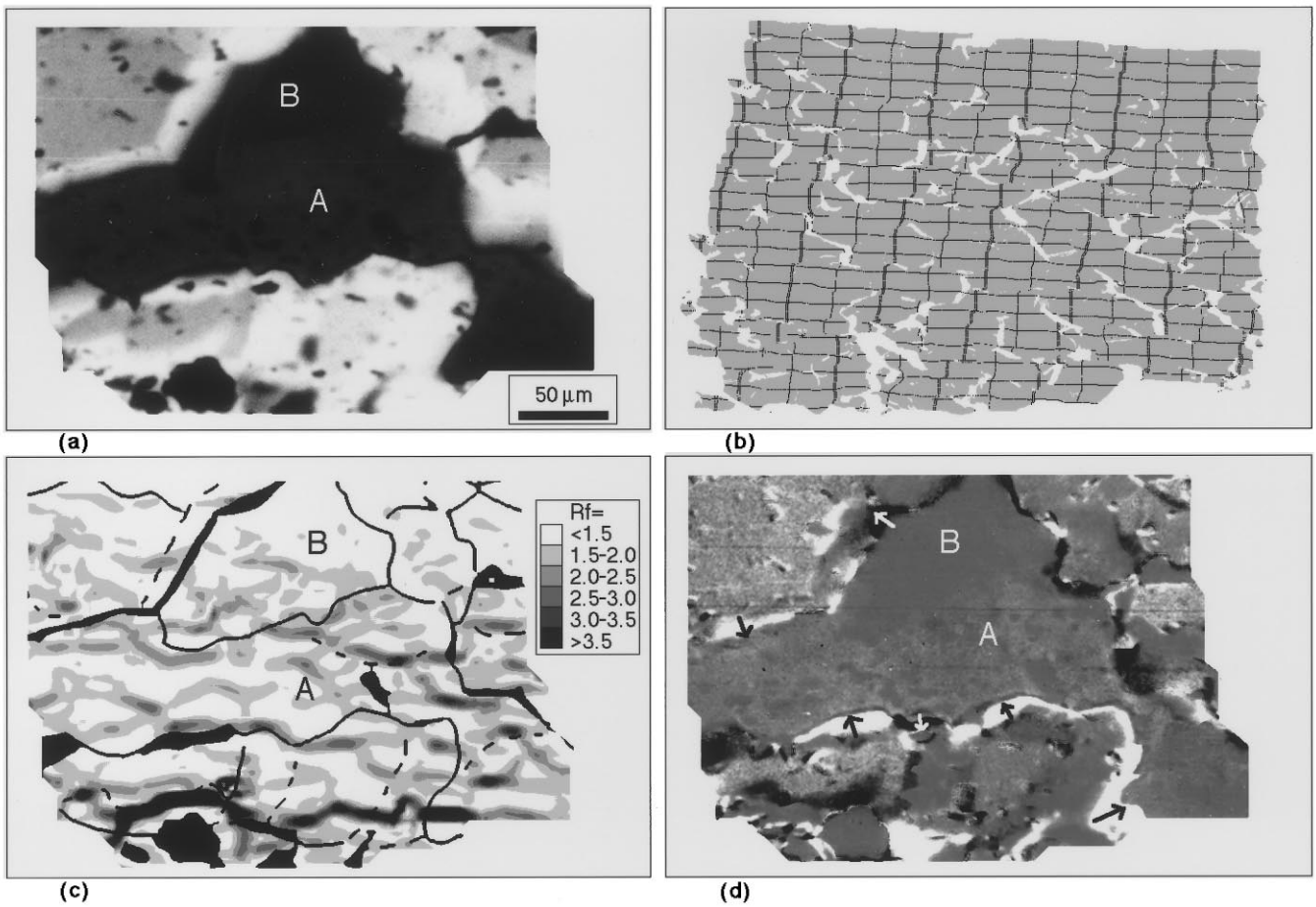

Fig. 4. Analysis of a small area around grains A and B in Fig. 2. (a) Selected area at the beginning of the strain increment of 8 min. (b) Deformed grid showing discrete steps in the off-set of vertical grid lines. (c) Overlay of grain boundaries (black) and contours of R_f values (calculated with a 20×20 pixel window). Dark bands are highest strain rate micro-shear zones. (d) Image showing the difference between the cross-polarised light image before and after the deformation increment. The deformed state image was 'back-strained' using the calculated displacement field. Differences between the two images are due to grain boundary migration (dark and light bands along grain boundaries) or changes in crystallographic orientation with respect to polars.

apparent volume loss zones, would be randomly distributed. Such apparent or 'false' dilatant zones may occur in the sample, but we can also see a regular pattern of the dilatant zones in Fig. 4(b). Such regular patterns were also observed in similar experiments by Sim (1997), who observed a preferred orientation of dilatant zones normal to the extension direction and volume loss zones normal to the shortening direction. We are therefore confident that these dilatant zones are real zones of material gain due to diffusional material transfer.

The transport path can either be lattice diffusion through the OCP grains or diffusion along grain boundaries and the OCP/glass interface. Micro-shearing and diffusional mass transfer probably constitute mutually accommodating deformation mechanisms. The relative amount of strain accommodated by micro-shearing can be estimated from the offsets of the vertical grid lines. Up to 75% of the total displacement difference (i.e. shear strain) across the image has taken place in the micro-shear zones. An overlay of grain boundaries (drawn in black) and micro-shear zones is shown in Fig. 4(c). The three most prominent micro-shear zones are at the base of the image, at the lower edge of grain A and between grains A and B, cutting through the upper right corner of grain A.

The arithmetic difference between the image of the undeformed state and the back-strained deformed state is shown in Fig. 4(d) in order to visualise the grain-boundary migration and change in birefringence. Grain-boundary migration of light grains at the expense of dark grains shows up as white bands (black arrows at lower edge of grain A). The opposite shows up as black bands. One can see that grain A is mostly shrinking, whereas grain B grows, but the boundary between grains A and B shows no movement. Differences in shading inside grains are due to changes in lattice orientation.

3.2. Discussion

The detailed strain analysis of the OCP experiment over a small strain increment shows that strong localisation of deformation occurs at the sub-grain and grain scales. The sites of localisation cannot be determined from the microstructure at the end of the deformation history. Two factors are causing this: dynamic recrystallisation and ongoing deformation. Together, these erase all or most traces of earlier deformation. More importantly, the sites of localisation vary during progressive deformation due to intracrystalline deformation between the micro-shear zones and recrystallisation. Grain-boundary mobility is high in OCP and grain boundaries constantly migrate through the material. Furthermore, recrystallisation leads to the formation and destruction of sub-grains and grains. As the (sub) grain-boundary network changes, so must the micro-shear zone network, since these micro-shear zones are preferentially located at grain and sub-grain boundaries. As a result, the micro-shear zones continuously come into existence, migrate through the material and disappear again. At any one instant a significant proportion (up to 75% here) of the deformation is localised in only a small proportion of the material. The sites of localisation vary with time and, over a large strain increment, all material may accumulate an equal amount of finite strain. The microstructures in naturally deformed rocks only show the effect of the accumulated deformation during the whole deformation event. Localisation as observed in these experiments is not necessarily observed in real tectonites if it did occur.

An important question is: do the observed small scale shear zones actually occur in naturally deforming rocks and are they important? This question is hard to answer if indicative microstructures are lacking. We argue here that the answer is probably affirmative on the following grounds:

(i) Shear localisation is observed at all scales where localisation leaves permanent traces in the structure. The lack of microstructural evidence for small scale shear localisation may be the result of the absence or destruction of indicative structures at these small scales rather than the absence of shear localisation.

(ii) Rocks are heterogeneous materials, even at the grain scale, resulting from variations in mineralogy, crystallographic orientation, grain size and dislocation density. Combined with a usually non-linear relationship between strain rate and stress down to the single slip-plane scale, this makes homogeneous deformation highly unlikely.

(iii) Although the OCP used in our study is not a rock-forming mineral, it has proved to be analogous to rock-forming minerals in its rheological behaviour and resulting microstructures. It is improbable that its behaviour should only be significantly different to that of real rocks in the particular aspect of shear localisation. Micro-shearing has also been reported in other analogue materials, such as norcamphor (Herwegh and Handy, 1996), high temperature OCP (Ree, 1994), magnesium/aluminium alloys and sodium nitrate (Drury and Humphreys, 1986, 1988). A difference with the results of Drury and Humphreys (1986, 1988) is that in their experiments the micro-shearing contributed less that 15% to the total strain and that it, combined with recrystallisation, produced a distinct microstructure of serrated grain boundaries.

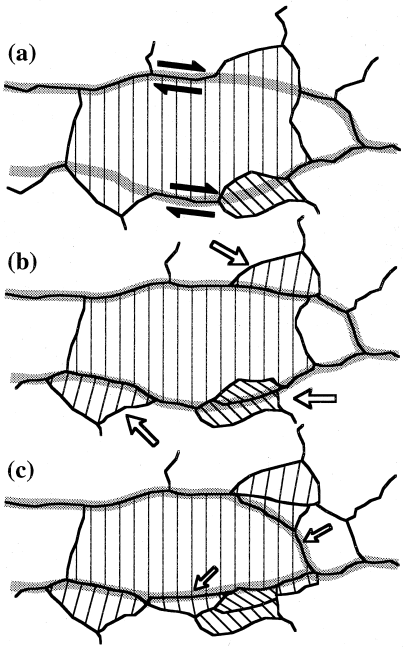

Fig. 5. Schematic drawing of how micro-shear zones may lead to progressive sub-grain rotation at the edges of grains. (a) Anastomosing micro-shear zones are preferentially located at grain boundaries but may dissect bulges. (b) Sliding of the cut-off parts of the grain may lead to slight rotation of the lattice resulting in the formation of sub-grains (arrows). (c) Micro-shear zones shift through the material (arrows), which leads to the formation of more and more sub-grains, especially at the margins of grains.

It would of course be desirable to find positive proof in the form of microstructures that can be preserved in (moderately) deformed rocks. Possible candidates are core–mantle structures. The progressive misorientation of sub-grains from core to mantle is usually interpreted as being caused by dislocation creep and recovery (White, 1977; Drury and Humphreys, 1986; Urai et al., 1986). Alternatively, these structures can be formed or modified by micro-shear zones in the following way (Fig. 5): A micro-shear zone may dissect a grain. The shear along the anastomosing micro-shear zones causes some passive rotation of the lenses in between the micro-shear zones. The amount of rotation differs from lens to lens resulting in a progressive angular mismatch between the lattices of the two parts of the dissected grain. Micro-shear zones are preferentially located at grain boundaries and will therefore usually only cut off small parts of grains, for instance corners or bulges. Continuous dissection causes more and more sub-grains to be formed with a progressive mismatch in lattice orientation from the core to the rim, producing the typical core–mantle structure. Such a mechanism was proposed by Nyman et al. (1992) for amphiboles, but may well apply to other minerals. It should be stressed that dislocation creep and recovery can produce the same microstructure and that the two mechanisms may operate together. This model is similar to the model of Drury and Humphreys (1986), where grain-boundary sliding is minor and only occurs at low strains until grain-boundary bulges inhibit further sliding. Our observations suggest that these bulges are cut off from the mother grain to allow continued sliding.

The apparent absence of indicative microstructures for small scale shear localisation may lead to erroneous interpretations of the mechanisms involved in the deformation. For instance, a strong crystallographic preferred orientation characterises the microstructure of Fig. 2. One could infer from this that dislocation creep was the only or main deformation mechanism operating during deformation. In reality this mechanism accommodated only part of the deformation ($<25\%$). A wrong, or only partly correct, assessment of the deformation mechanism may in turn lead to errors in the estimate of the rheological properties of the material. It is therefore important that the possible activity of micro-shear zones in real tectonites is taken into account and that we try to define indicators that may prove or disprove such activity. Careful (re)examination of real microstructures may enable us to do so and further experiments with rock analogues, such as presented here, can tell us what to look for.

4. Large scale localisation controlled by the experimental boundary conditions

In the circular shear zone experiments described here, the shear stress decreases outwards. One therefore expects the shear-strain rate to be highest at the inner grip of the shear zone and decrease outwards. This phenomenon was described by Masuda et al. (1995), who showed that the effect can be quite pronounced for power-law creep materials, such as OCP. Localisation of shear at the inner grip is indeed commonly observed in experiments (Jessell and Lister, 1991; ten Brink and Passchier, 1995). However, one also usually finds localisation of shear at the outer grip (Fig. 6) or in straight shear zones at one or both of the edges. This localisation cannot be explained with the radial dependence of shear stress as described by Masuda et al. (1995).

The analysis we present here suggests that the friction between the sample surface and the confining glass plates is the cause for the shear localisation at both edges of the shear zones in deformation cells. Shear stress parallel to the shear plane has to be transmitted from the grips through a very thin sample. The sample is sandwiched between glass plates that move at different speeds compared to the sample. Any sliding friction between sample surface and glass dissipates

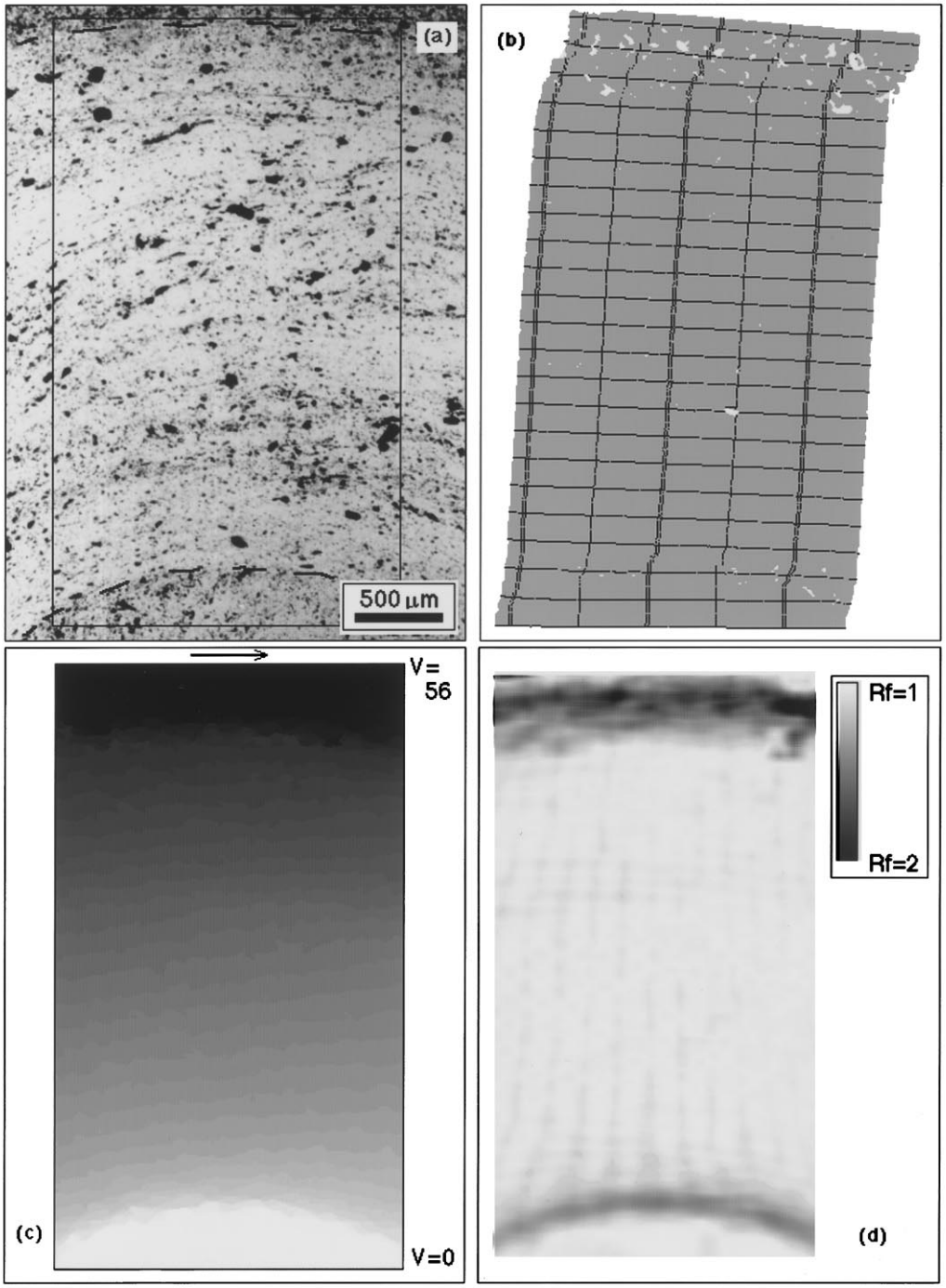

Fig. 6. Analysis of the distribution of deformation over the whole shear zone in the transparent deformation cell. (a) Plane polarised light image of the studied area. The inner (below) and outer grip edges (top) are drawn as dashed lines. (b) Deformed grid showing the displacement of material points across the shear zone over a time interval of 5 min. Most deformation is localised at the edges of the shear zone, especially the outer edge. (c) Grey scale plot of the horizontal (≈tangential) component of the displacement vectors, which range from 0 pixels (white) at the inner grip to 56 pixels (black) to the right at the outer grip. (d) Grey scale plot of R_f-values ranging from 1 (white) to almost 2 (black) at the edges of the shear zone. The values were calculated for a 20×20 pixel window around each individual pixel. Rounding-off of displacements to whole numbers (pixels) causes the vertical bands and should not be confused with micro-shear zones.

the shear stress away from the grips. Even though the sliding friction may be small, it acts on a much larger area (typically 1–3 mm wide) than the <100 µm wide area across which the shear stress has to be transmitted. The effective shear stress acting on the sample is therefore lowest in the middle of the shear zone. The effect of friction on the shear-strain rate profile cannot be determined analytically for a circular shear zone

where the rheology of the sample material and the friction behaviour are non-linear. One can determine the friction-induced shear localisation numerically, as is shown below.

The frictional stress (σ) due to sliding of OCP along a glass surface can be approximated with a power-law equation (Appendix A):

$$\sigma = B \cdot (v_{(\text{plate})} - v_{(\text{sample})})^m \tag{2}$$

with $B = 8.45$ [MPa m$^{-0.313}$ s$^{0.313}$] and $m = 0.313$, and v = velocity [m s^{-1}]. The flow law for OCP in simple shear is also a power-law (Bons and Urai, 1994):

$$\gamma = A \cdot \tau^n \tag{3}$$

with γ being the shear-strain rate, A a material constant, τ the shear stress and n the stress exponent ($A = 0.04$ [s^{-1} MPa$^{-4.5}$] and $n = 4.5$ for OCP at 30°C). The following derivation is for the case that the bottom glass plate, with the inner grip with radius $r = R_{\text{in}}$, has an angular velocity of ω_{in}. The outer grip, with radius $r = R_{\text{out}}$, on the top glass plate has an angular velocity of ω_{out}. The sample has a thickness of w. Let us suppose we know the angular velocity and shear stress at a point r and want to determine both at a point $r + \Delta r$. For the angular velocity we get, using $\omega = v/r$ and $\gamma = (\partial\omega/\partial r) \cdot r$:

$$\omega_{(r+\Delta r)} = \omega_{(r)} + (\mathrm{d}\omega/\mathrm{d}r)_{(r)} \cdot \Delta r = \omega_{(r)} + \frac{\gamma_{(r)} \cdot \Delta r}{r + \Delta r/2}$$

$$= \omega_{(r)} + \frac{A \cdot \tau_{(r)}^n \cdot \Delta r}{r + \Delta r/2}. \tag{4}$$

The shear stress changes with radius because of the frictional dissipation and the change in area on which the shear force acts:

$$\tau_{(r+\Delta r)} = \frac{r}{r + \Delta r}\left(\tau_{(r)} + \frac{\Delta r}{w}(B(\omega_{\text{out}} \cdot r - \omega_{(r)} \cdot r)^m - B(\omega_{(r)} \cdot r - \omega_{\text{in}} \cdot r)^m)\right). \tag{5}$$

Starting at $r = R_{\text{in}}$, where ω_{in} is known, r is increased to R_{out} by many small increments of Δr. However, the applied shear stress at R_{in} is usually not known. The correct value of $\tau_{(R_{\text{in}})}$, the one which gives the known value for ω_{out}, is determined iteratively.

Fig. 7 shows a comparison between the velocity and shear-strain rate profiles measured in the experiment and the calculated profile for a sample thickness of $w = 50$ μm. The calculated profile coincides reasonably well with the actual measurements, suggesting that the shear localisation at both edges of the shear zone can indeed be adequately explained by friction along the OCP–glass surface, but not by the radial dependence of shear-strain rate of Masuda et al. (1995) alone.

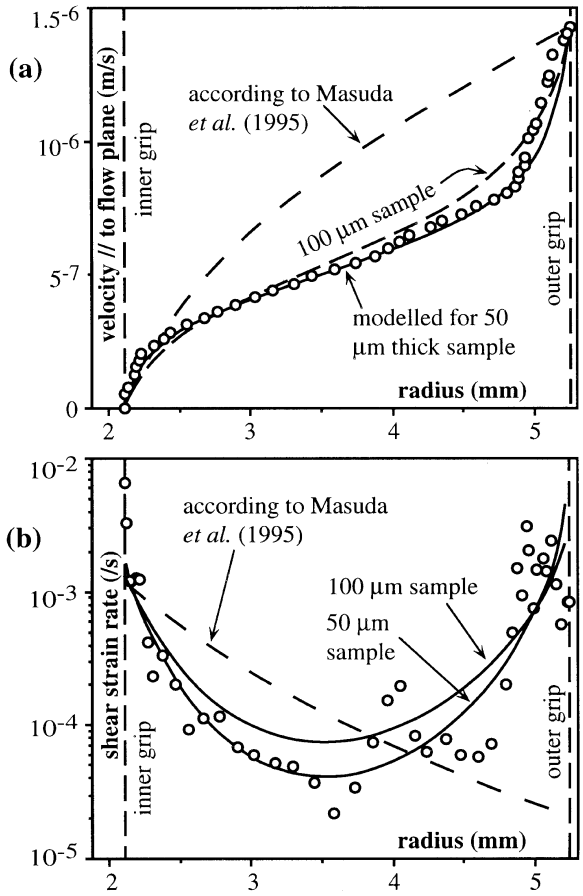

Fig. 7. Comparison of the actual shear profile across a shear zone in a transparent deformation cell and model predictions. (a) Velocity parallel to the flow plane as a function of radial distance from the centre of rotation. (b) Shear-strain rate profile. Open circles are velocities measured in the experiment (Fig. 6). The dashed line is for the model that only takes into account the radial dependence of the shear stress (Masuda et al., 1995). The closed lines also take friction along the glass plates into account and are calculated with the numerical method described in this paper, for a 50 and 100 μm thick OCP sample. One can see that friction along the glass plates is needed to explain the general shear profile with shear localisation at both edges of the shear zone.

It is clear that the shear localisation at the edges of the shear zone in transparent deformation cells can be entirely an artefact of the experimental method and has little geological relevance. Jessell and Lister (1991) discussed shear localisation near the inner grip in a circular shear zone and related it to shear-strain rate related grain size. However, they ignored the effect of friction. Shear profiles are different for different applied shear-strain rates, due to the non-linearity of the rheology of OCP and the frictional behaviour. Fig. 8 shows the magnitude of localisation relative to the case where there is no friction for different applied shear-strain rates. One can see that the localisation is most pronounced at a high applied shear-strain rate, which was also observed by Jessell and Lister (1991).

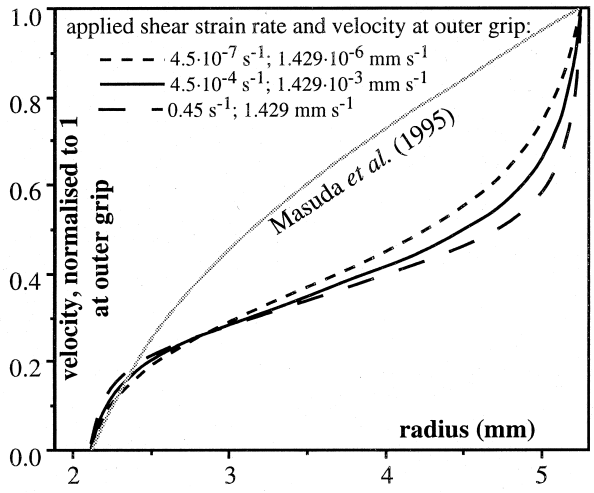

Fig. 8. Modelled velocity profiles in 50 μm thick OCP samples across a shear zone in a transparent deformation cell for different applied velocities at the outer grip. To facilitate the comparison, the velocities are normalised to unity at the outer edge of the shear zone. Applied velocities are the same as in the experiment shown in Fig. 6 (closed line), 1000 times faster (long dashes) and 1000 times slower (short dashes). Localisation at the edges of the shear zone is most pronounced at the highest applied shear-strain rate. The prediction by Masuda et al. (1995) is shown for comparison.

However, the time dependent localisation observed by them is not explained here.

We explained the localisation at the edges of our experimental shear zone as an artefact of the experimental geometry. This type of shear localisation looks similar to localisation found at rheological boundaries in naturally deformed rocks. Despite the similarity, the two should not be confused. The main difference is that, in natural rocks, stresses are transmitted across general parallel interfaces between layers and units of different rheology, whereas, in the experiments, stress is applied by glass plates that are normal to the shear zone. The effect of friction should be carefully considered in any deformation experiment in a deformation cell of the type discussed here. If the effect is unwanted, ways should be sought to minimise friction. In any case, the effect should be quantified as much as possible. The earlier equations may help in this.

5. Conclusions

Although a strong crystallographic preferred orientation suggested dislocation creep as the main deformation mechanism, it was found that a combination of displacement along micro-shear zones and diffusional creep accounted for 75% of the deformation in a sample of OCP. Narrow anastomosing micro-shear zones are preferentially located on grain and sub-grain boundaries. Lenses smaller than a grain to several grains in size are displaced along these micro-shear zones and these deform internally by intracrystalline deformation mechanisms. The micro-shear zones migrate through the material and leave no visible traces in the microstructure. Micro-shear zones may also operate in naturally deforming rocks, but the lack of indicative microstructures makes this difficult to prove. An alternative mechanism is given for the formation of core–mantle structures, based on the activity of micro-shear zones. These structures may be the only ones in which the activity of micro-shear zones leaves visible traces.

In transparent deformation cell experiments shear almost inevitably localises at the edges of the shear zone due to friction between the sample and the confining glass plates. A numerical solution to quantify this effect is given.

Acknowledgements

This work would not have been achieved without encouragement from, and discussions with Janos Urai and Coen ten Brink. The reviewers W.D. Means and J.G. Spray are thanked for their many comments and suggestions. Paul Bons acknowledges the previous financial support from the Netherlands Organisation for Scientific Research (NWO), the Australian Research Council (ARC) and, currently, from Monash University through a Logan Fellowship.

Appendix A

A simple experiment was carried out to estimate the frictional behaviour of OCP sliding along glass. A sample of OCP, measuring $10\times20\times0.5$ mm^3 was sandwiched between two glass plates (Fig. 9). The lower glass plate had a frosted surface and rested on a horizontal table surface. The upper plate had a smooth surface and rested completely on the piece of OCP. A weight was put on top of the upper glass plate to apply a normal stress on the glass–OCP surface. A shear stress (σ) on the glass–OCP contact surface was applied with a dead weight hanging on the upper glass plate with a wire that was led over a pulley. The horizontal displacement rate (v) of the upper glass plate as a result of this shear stress was measured with an LVDT over a total displacement distance of about 1.2 mm. Contact between glass and OCP was not complete and was estimated to be 1 cm^2. Eight tests were done with normal stresses of 0.4 and 0.6 MPa and shear stresses of 0.04, 0.08 and 0.18 MPa. The stresses acting on the sample also caused internal deformation of the sample, but the effect of this on the glass-displacement rate was determined to be negligible. Results

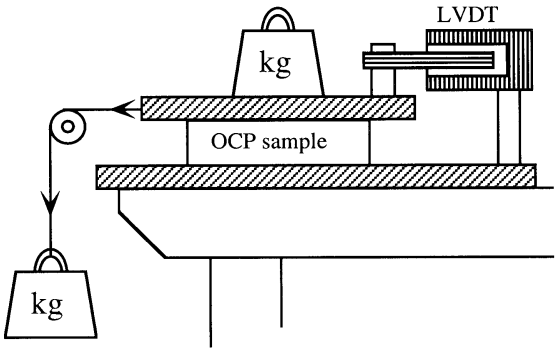

Fig. 9. Schematic drawing of the set-up used to determine the frictional behaviour of glass sliding over an OCP-surface as discussed in

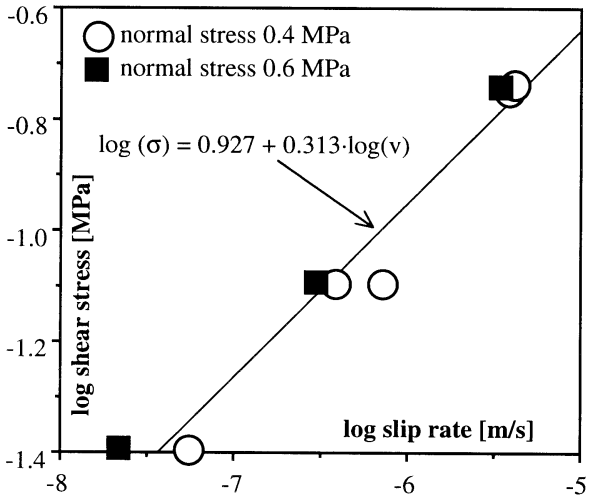

Fig. 10. Logarithmic plot of the relation between the shear stress and the slip rate along a glass–OCP surface. Normal stress on the contact surface was 0.4 and 0.6 MPa. The linear regression through all 8 data points was used in the model calculations for Figs. 7 and 8.

are shown in Fig. 10 in the form of a $\log(v)$–$\log(\sigma)$ plot. Although there is a slight difference between the data for 0.4 and 0.6 MPa, a linear regression was made through all eight data points, resulting in:

$$\log(\sigma) = 0.92689 + 0.31305 \cdot \log(v) \Leftrightarrow \sigma = 8.45 \cdot v^{0.313}. \quad \text{(A1)}$$

References

Berthé, D., Choukroune, P., Jegouzo, P., 1979. Orthogneiss, mylonite and non-coaxial deformation of granites: the example from the South Armoricain shear zone. Journal of Structural Geology 1, 31–42.

Bons, P.D., Jessell, M.W., 1995. Strain analysis in deformation experiments with pattern matching or a stereoscope. Journal of Structural Geology 17, 915–921.

Bons, P.D., Urai, J.L., 1992. Syndeformational grain growth: microstructures and kinetics. Journal of Structural Geology 14, 1101–1109.

Bons, P.D., Urai, J.L., 1994. Experimental deformation of two-phase rock analogues. Materials Science and Engineering A175, 221–230.

Bons, P.D., Jessell, M.W., Passchier, C.W., 1993. The analysis of progressive deformation in rock analogues. Journal of Structural Geology 15, 403–412.

Drury, M.R., Humphreys, F.J., 1986. The development of microstructure in Al–5% Mg during high temperature deformation. Acta Metallurgica 34, 2259–2271.

Drury, M.R., Humphreys, F.J., 1988. Microstructural shear criteria associated with grain-boundary sliding during ductile deformation. Journal of Structural Geology 10, 83–89.

Drury, M.R., Humphreys, F.J., White, S.H., 1985. Large strain deformation studies using polycrystalline magnesium as a rock analogue. Part II: dynamic recrystallisation mechanisms at high temperatures. Physics of Earth and Planetary Interiors 40, 208–222.

Gapais, D., White, S.H., 1982. Ductile shear bands in naturally deformed quartzite. Textures and Microstructures 5, 1–17.

Hanmer, S., Passchier, C.W., 1991. Shear sense indicators: a review. Geological Survey of Canada Paper 90, 1–71.

Herwegh, M., Handy, M.R., 1996. The evolution of high temperature mylonitic microfabrics: evidence from simple shearing of a quartz analogue (Norcamphor). Journal of Structural Geology 18, 689–710.

Hobbs, B.E., Ord, A., 1988. Plastic instabilities: implications for the origin of intermediate and deep focus earthquakes. Journal of Geophysical Research 93, 10,521–10,540.

Hobbs, B.E., Ord, A., Teyssier, C., 1986. Earthquakes in the ductile regime? Pure and Applied Geophysics 124, 309–336.

Ishii, K., 1992. Partitioning of non-coaxiality in deforming layered rock masses. Tectonophysics 210, 33–43.

Jessell, M.W., 1986. Grain boundary migration and fabric development in experimentally deformed octachloropropane. Journal of Structural Geology 8, 527–542.

Jessell, M.W., Lister, G.S., 1991. Strain localization behaviour in experimental shear zones. Pure and Applied Geophysics 137, 421–438.

Lister, G.S., Snoke, A.W., 1984. *S–C* mylonites. Journal of Structural Geology 6, 617–638.

Mancktelow, N.S., 1991. The analysis of progressive deformation from an inscribed grid. Journal of Structural Geology 13, 859–864.

Masuda, T., Mizuno, N., Kobayashi, M., Nam, T., Otoh, S., 1995. Stress and strain estimates for Newtonian and non-Newtonian materials in a rotational shear zone. Journal of Structural Geology 17, 451–454.

McCrone, W.C., Cheng, P.T., 1949. Grain growth in octachloropropane. Journal of Applied Physics 20, 230–231.

Means, W.D., 1981. The concept of steady-state foliation. Tectonophysics 78, 179–199.

Means, W.D., 1989. Synkinematic microscopy of transparent polycrystals. Journal of Structural Geology 11, 163–174.

Means, W.D., 1990. Kinematics, stress, deformation and material behaviour. Journal of Structural Geology 12, 953–971.

Nyman, M.W., Law, R.D., Smelik, E.A., 1992. Cataclastic deformation mechanism for the development of core–mantle structures in amphibole. Geology 20, 455–458.

Passchier, C.W., 1988. Analysis of deformation paths in shear zones. Geologische Rundschau 77, 309–318.

Platt, J.P., 1984. Secondary cleavages in ductile shear zones. Journal of Structural Geology 6, 439–442.

Platt, J.P., Vissers, R.L.M., 1980. Extensional structures in anisotropic rocks. Journal of Structural Geology 2, 397–410.

Poirier, J.P., 1980. Shear localization and shear instability in materials in the ductile field. Journal of Structural Geology 2, 135–142.

Ramberg, H., 1975. Particle paths, displacements and progressive strain applicable to rocks. Tectonophysics 28, 1–37.

Ree, J.H., 1991. An experimental steady-state foliation. Journal of Structural Geology 13, 1001–1011.

Ree, J.H., 1994. Grain boundary sliding and development of grain boundary openings in experimentally deformed octachloropropane. Journal of Structural Geology 16, 403–418.

Ree, J.H., Park, Y., 1997. Static recovery and recrystallization microstructures in sheared octachloropropane. Journal of Structural Geology 19, 1521–1526.

Sim, H.S., 1997. Small-scale localisation of deformation. BSc-Honours thesis, Monash University, Australia.

ten Brink, C.E., Passchier, C.W., 1995. Modelling of mantled porphyroclasts using rock analogue materials. Journal of Structural Geology 17, 131–146.

Urai, J., Means, W.D., Lister, G.S., 1986. Dynamic recrystallisation of minerals. In: Hobbs, B.E., Heard, H.C. (Eds.), Mineral and Rock Deformation: Laboratory Studies. The Paterson volume. Geophysical Monograph 36, pp. 161–200.

Wenk, H.-R., Kern, H., van Houtte, P., Wagner, F., 1986. Heterogeneous strain in axial deformation of limestone: textural evidence. In: Hobbs, B.E., Heard, H.C. (Eds.), Mineral and Rock Deformation: Laboratory Studies. The Paterson volume. Geophysical Monograph 36, pp. 287–295.

White, S.H., 1977. Geological significance of recovery and recrystallization processes in quartz. Tectonophysics 39, 613–628.

White, S.H., Burrows, S.E., Carreras, J., Shaw, N.D., Humphreys, F.J., 1980. On mylonites in ductile shear zones. Journal of Structural Geology 2, 175–187.